Diffusion of oxygen vacancies on a strained rutile TiO_2(110) surface

Zhao-Wu Wang, Da-Jun Shu,* Mu Wang,† and Nai-Ben Ming
National Laboratory of Solid State Microstructures and Department of Physics, Nanjing University, Nanjing 210093, China
(Received 30 April 2010; revised manuscript received 14 September 2010; published 6 October 2010)

Based on first-principles calculations of the rutile TiO_2(110) surface with different types of oxygen vacancies, a *phase diagram* is constructed for the energetically favorable oxygen vacancy as a function of the externally applied in-plane strain. When the strain is relatively small, the bridging oxygen vacancy (BOV) is the energetically favorable one. The pathways and the energy barriers of surface diffusion of the BOV under different external strain are studied. For the cross row diffusion of the BOV along $[1\bar{1}0]$, a concerted diffusion mechanism mediated by the in-plane oxygen vacancy is found to be energetically more favorable than the hopping diffusion. The energy barrier of the concerted diffusion along $[1\bar{1}0]$ and that of the hopping diffusion along [001] are found to decrease with increasing strain. The former decreases more dramatically than the latter when the strain is applied along $[1\bar{1}0]$, which suggests a possible way of facilitating the diffusion anisotropy.

DOI: 10.1103/PhysRevB.82.165309 PACS number(s): 68.47.Gh, 68.35.Dv, 68.35.Gy, 68.35.Md

I. INTRODUCTION

In recent years, much attention has been paid to the surfaces of titanium dioxide due to their promising applications in heterogeneous catalysis, solar cells, gas sensor, photocatalysis, cleaning environment, etc.[1–5] It has been widely reported that oxygen vacancies (OVs) are the most common defects on TiO_2 surfaces and play critical roles in the surface reactions.[6–13] If one can control and change the type and the distribution of oxygen vacancies, the surface reaction properties can be accordingly modified. For this purpose, one needs to understand both the influence of oxygen vacancies on the surface properties and the responses of oxygen vacancies to different external fields.[14,15]

External strain is unavoidable especially in the fabrication of nanostructures and thin films.[16,17] The responses of a nanostructure to the external strain are largely determined by its surface mechanical properties, which are influenced by the type and distribution of the surface defects.[18–21] Recently we have found by first-principles calculations that rutile TiO_2(110) surface with different types of oxygen vacancies possesses different surface mechanical properties, therefore the type of the energetically favorable oxygen vacancies (EFOV) can be tuned by applying different strain to the system.[22]

In addition to the energetics, the surface kinetics properties of the oxygen vacancies also influence their distribution. It has been reported that OVs on rutile TiO_2(110) surface diffuse more easily along the surface oxygen row in the [001] direction than across the oxygen row.[23,24] In order to engineer the surface properties by external strain, it is important to understand the diffusion properties of the surface OVs under different state of externally applied strain. For surface adatoms, we have demonstrated a simple method for predicting quantitatively how an external strain will change the surface diffusion based on the knowledge of surface-stress tensors of the unstrained surface.[25] In comparison, it is worthy to check whether the method is still applicable for the diffusion of surface vacancies on oxide surfaces.

In this paper, we study the formation energy of the three types of surface OVs under the biaxial strain. A *phase diagram* is constructed for the type of EFOV on the TiO_2(110) surface as a function of the in-plane strain. The diffusion properties of the bridging oxygen vacancy (BOV), which is the energetically favorable one when the external strain is relative small, are then explored under different externally applied strain. For the cross row diffusion of the BOV along $[1\bar{1}0]$, a concerted diffusion mechanism mediated by the in-plane oxygen vacancy is found to be energetically more favorable than the hopping mechanism. Both the energy barrier of the concerted diffusion along $[1\bar{1}0]$ and that of the hopping diffusion along [001] decrease with increasing tensile strain. When the tensile strain is applied along $[1\bar{1}0]$, the energy barrier of the concerted diffusion along $[1\bar{1}0]$ becomes much lower than that of the hopping diffusion along [001], which suggests a possible way of facilitating the cross row diffusion.

II. COMPUTATIONAL METHODS

The calculations are based on density functional theory in the PW91 generalized gradient approximation,[26] using the Vienna *ab initio* simulation package code with projector augmented wave pseudopotentials.[27,28] An energy cutoff of 396 eV is used for expanding the Kohn-Sham wave functions. The rutile TiO_2(110) surface is modeled as a (2×2) supercell consisting of a six-trilayer slab and a vacuum with thickness of five-trilayer. Monkhorst-Pack *k*-points grid[29] of $2\times4\times1$ is used, which has been tested to be well converged. The bottom two trilayers are fixed to mimic the bulk, and the relaxation is carried out until all forces on the free ions are converged to 0.01 eV/Å. Nudged elastic band (NEB) method is used to find the minimum energy paths and the transition states for diffusion of OVs on the rutile TiO_2(110) surface.[30]

The perfect rutile TiO_2(110) surface is shown in Fig. 1, which is characterized by rows of bridging oxygen atoms along the [001] direction, between which is a trough consisting of two symmetrical rows of in-plane oxygen atoms. There are three types of oxygen atoms in the first trilayer,

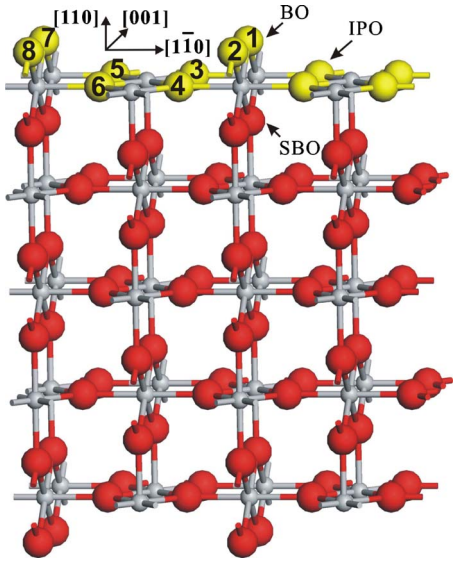

FIG. 1. (Color online) Schematic of the rutile $TiO_2(110)$ surface. Large spheres and small spheres indicate the O and Ti atoms, respectively. The oxygen atoms on the surface are marked as light color (yellow on line). The bridging oxygen, the sub-bridging oxygen and the in-plane oxygen are indicated by the arrows. The numbers label the different oxygen atoms on the surface in order for reference below.

i.e., the bridging oxygen, the in-plane oxygen and the sub-bridging oxygen atoms, as marked by the arrows in Fig. 1. Three types of surface OVs can be introduced correspondingly by removing different types of the surface oxygen atoms, termed as the bridging OV, the in-plane OV (IPOV) and the sub-bridging OV (SBOV), respectively. The OV density is thus $\theta=1/4$ per unit surface cell in all of our calculations.

In previous work we have shown that when the defect density decreases, the relative differences in the formation energy of different types of vacancies change little, although the absolute values do decrease.[22] In this work we check the energy barriers of different pathways using a (2×4) supercell ($\theta=1/8$). We find that the relative difference only decreases slightly. Therefore a (2×2) supercell is used to study the strain effect for the sake of computation efficiency.

III. FORMATION OF THE OXYGEN VACANCIES

The formation energy E_{OV} of an oxygen vacancy can be expressed as

$$E_{OV} = E_{vac} - E_{st} + \frac{1}{2}E_{O_2}, \tag{1}$$

where E_{st} and E_{vac} stand for the energy of the stoichiometric structure and that of the same structure except containing an OV, respectively, and E_{O_2} is the energy of an isolated O_2 molecule. We have considered previously the OV formation energy as a function of the uniaxially applied strain.[22] In this work, we apply the biaxial strain to the surface and study the formation energies of three types of surface OVs.

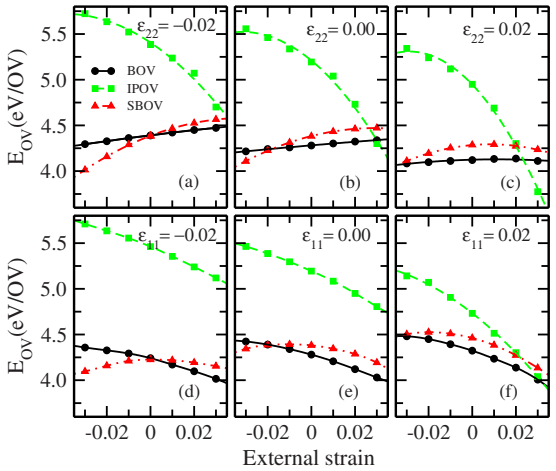

FIG. 2. (Color online) The OV formation energies as functions of the externally applied strain. The curves are quadratic fitted. ϵ_{11} and ϵ_{22} denote the strain along $[1\bar{1}0]$ and [001], respectively. The abscissa of the upper panels (a, b, and c) represent ϵ_{11} while that of the lower panels (d, e, and f) represent ϵ_{22}.

The formation energies of different types of OVs are calculated under biaxial strain in the range from −0.03 to +0.03, with positive and negative signs denoting the tensile and compressive strain, respectively. For comparison, the upper panels in Fig. 2 show the vacancy formation energies as functions of strain along $[1\bar{1}0]$ (ϵ_{11}) while the lower panels show the OV formation energies changing with strain along [001] (ϵ_{22}). It shows that the formation energy of IPOV decreases (increases) dramatically with tensile (compressive) strain along either direction. Contrarily, the formation energies of BOV and SBOV just change slightly with the external strain. Therefore the relative formation probabilities of different types of OVs depend on the specific externally applied strain field.

The interaction of external strain and oxygen vacancies is attributed to the dependence of surface elastic properties of rutile $TiO_2(110)$ on the type of oxygen vacancies. Surface stress tensor $\sigma_{\alpha\beta}$ and surface elastic constants $S_{\alpha\beta\alpha'\beta'}$ can be expressed as,[31,32]

$$\sigma_{\alpha\beta} = \frac{1}{A_L}\frac{\partial(A_L\gamma_L)}{\partial\epsilon_{\alpha\beta}} = \frac{\partial\gamma_L}{\partial\epsilon_{\alpha\beta}}$$

$$S_{\alpha\beta\alpha'\beta'} = \frac{\partial\sigma_{\alpha\beta}}{\partial\epsilon_{\alpha'\beta'}} = \frac{\partial^2\gamma_L}{\partial\epsilon_{\alpha\beta}\partial\epsilon_{\alpha'\beta'}}. \tag{2}$$

The indices α and β denote the two directions along the surface. A_L is the area of the surface in an unstrained state, and γ_L is the Lagrangian surface energy per unit area in an unstrained state.

In order to obtain the influence of oxygen vacancies on the surface elasticity, one needs to first relate the vacancy-induced change in surface energy $\Delta\gamma$ to the strain-dependent OV formation energies as follows:

TABLE I. Changes in surface mechanical properties induced by different types of oxygen vacancies with density of $\theta=1/4$ per unit cell. The units are eV/(1×1). The subscripts 11 and 22 denote the directions along $[1\bar{1}0]$ and [001], respectively.

Oxygen vacancy	$\Delta\sigma_{11}$	$\Delta\sigma_{22}$	ΔS_{1111}	ΔS_{2222}	ΔS_{1122}
BOV	0.51	−1.66	−2.42	−29.36	−14.76
IPOV	−5.02	−2.73	−151.01	−34.03	−53.21
SBOV	1.50	−0.63	−51.67	−62.98	−44.09

$$\Delta\gamma=\frac{E_{\mathrm{vac}}-E_{\mathrm{st}}}{A_L}\equiv\theta\frac{E_{\mathrm{OV}}-\frac{1}{2}E_{\mathrm{O}_2}}{A_{L0}}, \tag{3}$$

where θ is the density of vacancies, A_{L0} is the area per unit surface cell. By substituting Eq. (3) into Eq. (2), we can derive the changes in the surface elastic properties induced by different types of surface OVs. The results are shown in Table I for OV density $\theta=1/4$ per unit surface cell. It is obvious that the IPOV induces the largest changes in the surface elastic properties, therefore the corresponding formation energy changes most dramatically with the external strain. Since biaxial strain is applied, we can now obtain the information of ΔS_{1122} in comparison with Table I in Ref. 22.

Since the formation energies of different types of OVs depends on the external strain, the type of EFOV changes with external strain, as reported before.[22] It shows that the energetically favorable oxygen vacancy is the bridging one when no strain is applied, which changes to IPOV (SBOV) when sufficient large tensile (compressive) strain is applied, respectively. If we define the type of EFOV as a *phase*, the *phase diagram* can be constructed as a function of the external strain ϵ_{11} and ϵ_{22} using the intersection points in Fig. 2, as shown by the discrete points in Fig. 3.

The phase diagram can also be predicted according to the surface mechanical properties. In second-order approximation, the change in the surface energy induced by the surface defect can be expressed as a function of external strain,

$$\Delta\gamma=\Delta\gamma_0+\epsilon_{11}\Delta\sigma_{11}+\epsilon_{22}\Delta\sigma_{22}+\frac{1}{2}\epsilon_{11}^2\Delta S_{1111}+\frac{1}{2}\epsilon_{22}^2\Delta S_{2222}+\epsilon_{11}\epsilon_{22}\Delta S_{1122}. \tag{4}$$

By substituting the data in Table. I into Eq. (4), $\Delta\gamma_{\mathrm{BOV}}$, $\Delta\gamma_{\mathrm{IPOV}}$, and $\Delta\gamma_{\mathrm{SBOV}}$ can be obtained for BOV, IPOV, and SBOV on the rutile $TiO_2(110)$ surface, respectively. By comparing the three quantities as functions of ϵ_{11} and ϵ_{22}, the transition curves of the EFOV type from one to the other are deduced. In this way the phase diagram is constructed, as shown by dashed lines in Fig. 3. It is obvious that the results of the two methods fit very well within the considered range of strain.

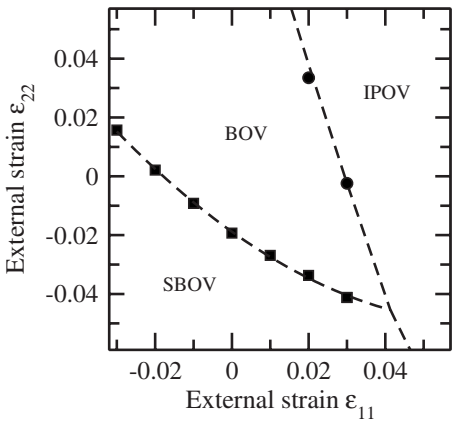

FIG. 3. Phase diagram of the type of EFOV as a function of the external strain ϵ_{11} and ϵ_{22}. The dashed curves are predicted according to the surface elasticity properties shown in Table I. It indicates that BOV, IPOV, or SBOV can be energetically most favorable within different range of the external strain.

The phase diagram is helpful for practical applications. For example, in growth of TiO_2 nanostructures on a specific substrate, the external strain can be exactly evaluated according to the lattice mismatch between TiO_2 and the substrate. Therefore one can choose suitable substrate in order to obtain the desirable EFOV according to the phase diagram.

IV. DIFFUSION OF THE BRIDGING OXYGEN VACANCY

The phase diagram shown in Fig. 3 indicates that the bridging OV is the energetically favorable one when the external strain is relatively small. Experimentally, it is also reported that BOVs are the most frequently observed one and play critical roles in surface reactions.[33,34] Therefore it is of essential importance to study the kinetic properties of BOVs.

It is known that surface diffusion properties correlate with the surface structures.[35] As shown in Fig. 1, the surface structure of the rutile $TiO_2(110)$ is anisotropic: Bridging oxygen atoms form rows along the [001] direction, between which is a trough consisting of two symmetrical rows of in-plane oxygen atoms. Correspondingly, the diffusion properties of BOV are expected to be also anisotropic. It is reported that the BOVs diffuse more easily along the [001] direction than across the oxygen rows along the $[00\bar{1}]$ direction.[23] In this work we consider the diffusion of the BOV along [001] and $[1\bar{1}0]$ under externally applied strain.

The BOV is initially created by removing the oxygen atom numbered one in Fig. 1. Along the oxygen row in the [001] direction, the BOV diffuses via hopping of the nearest neighbor oxygen atom numbered two (OA_2), as shown in Fig. 4. In the transition state shown in Fig. 4(c), OA_2 locates directly on top of the underlying six-coordinated Ti atom

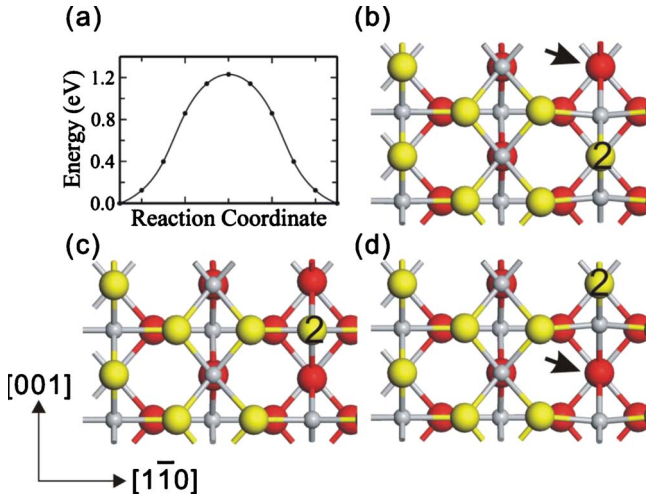

FIG. 4. (Color online) (a) The energy profile of the diffusion pathway of the BOV along the [001] direction via hopping mechanism (Path I). The zero points of the energy in all the energy profiles in this work is set to be the energy of the initial state. (b), (c), and (d) are the top views of the initial state, the transition state and the final states, respectively, with oxygen vacancies in the initial and final state marked with arrows. For clarity, only the hoping oxygen atom (OA_2) is numbered, The same representation as in Fig. 1 is used to distinguish the atoms.

(TA_{6c}). The energy profile of the pathway is calculated using the NEB method and is shown in Fig. 4(a). The energy barrier of 1.19 eV is consistent with the experimental value of 1.15 eV.[23] This diffusion pathway is referred hereafter as Path I.

The diffusion of the BOV along the [1$\bar{1}$0] direction via hopping of the oxygen atom numbered seven (OA_7) is shown in Fig. 5, referred hereafter as Path II. The state shown in Fig. 5(d) where OA_7 hops on top of the five-coordinated Ti atom (TA_{5c}) is found metastable. The diffusion barrier is determined as 2.55 eV using the NEB method, higher than that of Path I by 1.36 eV. Previously, larger energy barriers for the cross row hopping of the bridging oxygen atom are reported without calculation details.[23,33] In spite of the difference in the energy barrier, all the results suggest that the diffusion along [1$\bar{1}$0] via the hopping mechanism is energetically unfavorable.

In addition to the hopping mechanism, a concerted diffusion pathway is considered for BOV diffusing along the [1$\bar{1}$0] direction, which is referred hereafter as Path III. The concerted diffusion pathway is two stepwise. In the first step, the two original in-plane oxygen atoms OA_3 and OA_5 diffuse, until OA_3 hops to the original BOV site and OA_5 hops on top of the Ti atoms row [(b)–(d) in Fig. 6]. In the second step, OA_5 hops down to the in-plane oxygen site on the other side, meanwhile OA_7 hops to the nearby in-plane oxygen site. As a result, the oxygen vacancy diffuses by one surface lattice along [1$\bar{1}$0] [(d) and (f) in Fig. 6]. The transition state is shown in Fig. 6(d), in which a pair of IPOVs and an adatom coexist on the surface. Actually we find that when one in-plane atom, OA_3, for example, is removed from the rutile TiO_2(110), OA_5 always tends to climb on the Ti atoms

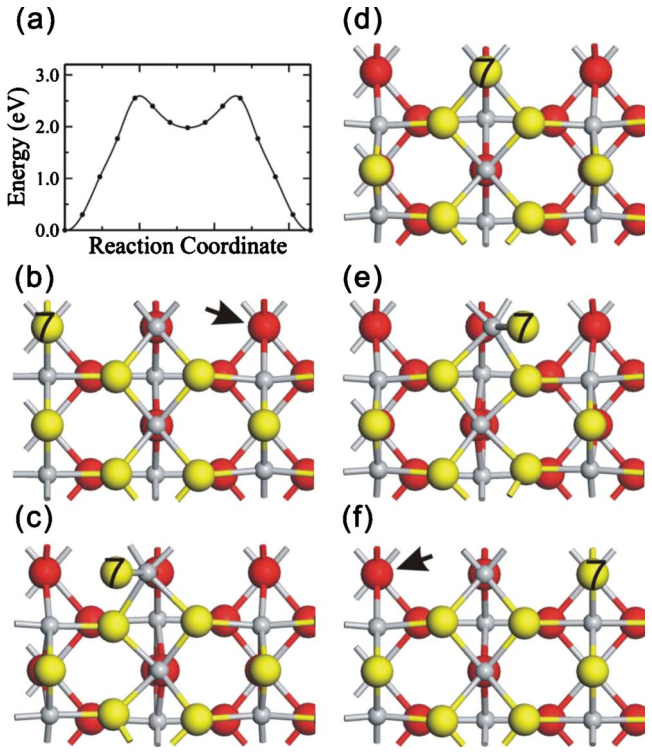

FIG. 5. (Color online) (a) The energetics of the diffusion pathway of the BOV along the [1$\bar{1}$0] direction via hopping mechanism (Path II). (b) and (f) are the top views of the initial and final states, with oxygen vacancies marked with arrows; (c) and (e) the two equivalent transition states, and (d) the metastable state. Only the hopping oxygen atom (OA_7) is numbered.

row with an energy gain of about 1.17 eV. It results in a pair of IPOVs plus an adatom, just as the transition state shown in Fig. 6(c). Therefore this concerted diffusion pathway can be regarded as mediated by a pair of IPOVs.

The energy profile of this pathway is given in Fig. 6(a), which indicates an energy barrier of 0.91 eV. It is worthy to mention that atoms in the transition state may not completely lose their memory about the history of movements. Therefore in the second step, there is a higher possibility for OA_5 to hop forward to the original position of OA_3 as shown in Figs. 6(e) and 6(f), than to hop backward to its own original position. If in this stage it is OA_8, i.e., the oxygen atom numbered eight in Fig. 6(b), instead of OA_7 that moves, the diagonal diffusion of OV is resulted. The concerted mechanism of the cross row diffusion bears comparative analogy to the exchange mechanism in homoepitaxial diffusion of an isolated adatom across the atomic rows on the (110) surface of a fcc metal.[35] Note that a similar concerted diffusion mechanism of BOV along [001], mediated by the nearby in-plane oxygen atom, is highly unfavorable due to a large energy barrier of 2.08 eV. It is reasonable since a single in-plane OV is unstable against forming a pair of in-plane OVs plus an adatom as discussed above.

It is well known that when the diffusion is thermally activated, the hopping rate of atoms at low temperature T can be described by the Arrhenius equation, $\nu \exp(-E_b/k_BT)$, where E_b is the energy barrier and k_B is the Boltzmann's

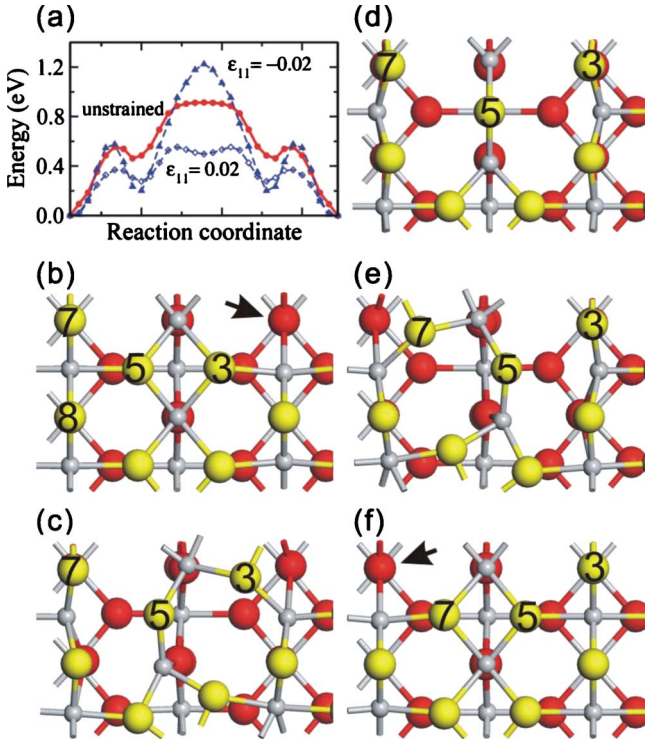

FIG. 6. (Color online) (a) The energy profile of the concerted diffusion pathway of the bridging OV along the $[1\bar{1}0]$ direction (Path III) when ϵ=0 and $\epsilon_{11}=\pm 0.02$. (b) and (f) are the top views of the initial and final states when no strain is applied, with oxygen vacancies marked with arrows; (c) and (e) the metastable states, and (d) the transition state. From (b) to (d), OA_3 and OA_5 are the moving surface atoms. From (d) to (f), OA_5 and OA_7 move.

constant,[35] and ν is the prefactor which can be interpreted as an attempt frequency. By comparison of the energy barriers, it is obvious that it is less efficient for a BOV to diffuse via hopping mechanism across the bridging oxygen row than along the row. However, cross-row diffusion of the BOV can be possible via concerted motion of the oxygen atoms, considering the relative low energy barrier of 0.91 eV in comparison with that of 1.19 eV for the diffusion along [001].

In order to estimate the prefactors ν, we have calculated the vibration frequencies of surface bridging oxygen along $[1\bar{1}0]$ and [001], with the results of 7.08 THz and 14.16 THz, respectively. Previous reports showed that comprehensive calculations may modify the prefactor by several times, yet the prefactor usually be in the order of magnitude of $10^{-1}-10$ THz.[36,37] Even in the very unfavorable case when ν is 0.1 Thz and 100 Thz for the cross-row concerted diffusion and the diffusion along the row, respectively, the cross-row concerted diffusion is still more efficient than the along-row diffusion at temperature below 470 K. Experimentally, we just find one work on BOV diffusion on this surface, in which only diffusion along [001] direction is detected.[23] Here we suggest that further experiments be conducted in order to explore the vacancy diffusion mechanism.

Now we apply external strain to the system and study the responses of the diffusion properties to the strain. Along the [001] direction, diffusion mechanism via single atom hopping is considered (Path I) while along $[1\bar{1}0]$, we just consider the concerted diffusion mechanism due to its lower barrier (Path III). The NEB method is used to obtain the energy profiles under different strain states. We find that either tensile strain or compressive strain does not change the topology of the energy profile of Path I, except with a slightly different energy barrier. The situation is different for Path III, of which typical energy profiles under externally applied strain are shown in Fig. 6(a). The saddle point in the unstrained state remains to be a saddle point under compressive strain whereas under tensile strain it becomes metastable and the new transition states occur nearby symmetrically. In this case the energy barrier actually corresponds to the one from BOV to IPOV. Note that for larger tensile strain when IPOV is more stable than BOV, the energy barrier from BOV to IPOV is lower than the one from IPOV to BOV.

In our previous work it has been demonstrated that when an adatom diffuses on a surface under the applied strain, the effect of the strain on diffusion is correlated with the intrinsic surface stress induced by the adatom along the diffusion pathways.[25] Since BOV diffusion is actually a consequence of diffusion of the neighboring surface oxygen atoms, surface stress also varies during the diffusion process. Therefore one can predict the dependence of diffusion barrier on the external strain based on the difference of the intrinsic surface stress tensor of the saddle point and the minimum point $\Delta\sigma$,

$$E_b = E_b^0 + A_L(\Delta\sigma)\epsilon. \tag{5}$$

For a complicated diffusion pathway, however, the transition state may vary under strain, as discussed above for the concerted diffusion along Path III. Therefore Eq. (5) does not apply in this case. Here we demonstrate that for such kind of complicated diffusion, one can also predict the energy profile of the pathway under applied strain as follows:

$$E_i = E_i^0 + A_L[(\sigma_{11}^i - \sigma_{11}^0)\epsilon_{11} + (\sigma_{22}^i - \sigma_{22}^0)\epsilon_{22}] = E_i^0 + A_L\Delta\sigma^i\epsilon, \tag{6}$$

where σ^i is the intrinsic surface-stress tensors at the ith configuration along the diffusion pathway.

Based on the variation in the surface stress tensor versus the reaction coordinate, the predicted energy profiles of Path III under strain are calculated and shown as curves in Figs. 7(a) and 7(b). To compare, the calculated energy profiles using NEB method are also shown as discrete points for ϵ =0 and $\epsilon_{22}=\pm 0.02$. It is obvious that the prediction can correctly give the topological changes in the energy profiles under different strain state. As shown in Fig. 7(b), when the external strain is applied along [001], the calculated energy profile matches the prediction quite well even when ϵ_{22} is up to 2%, except for the relaxation of some configuration which leads to lower energy related to the predicted values. By comparing Figs. 6(a) and 7(a), it indicates that the prediction overestimates the energy profile a little bit when ϵ_{11} is 2%, which can be attributed to the larger room facilitating the elastic relaxation.

The energy barriers according to the profiles of energy of Path I and Path III are shown in Figs. 7(c) and 7(d), versus the external strain ϵ_{11} and ϵ_{22}, respectively. The diffusion

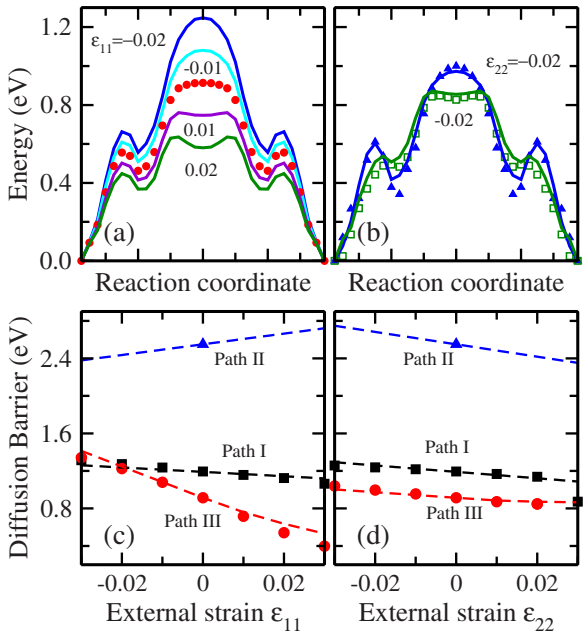

FIG. 7. (Color online) Upper panels: The predicted energy profiles of Path III under external strain along $[1\bar{1}0]$ (a) and [001] (b), according to Eq. (6). The calculated energy profiles using NEB method when $\epsilon=0$ (discrete circles), $\epsilon_{22}=-0.02$ (discrete triangles) and $\epsilon_{22}=0.02$ (discrete squares) are also shown for comparison. Lower panels: the diffusion barriers of different pathways as a function of the external strain, with discrete points and dashed lines denoting the calculated and predicted values, respectively.

barrier decreases with increasing strain, which suggests that the surface diffusion of BOVs can be facilitated by applying tensile strain in either direction. With increasing strain applied in the $[1\bar{1}0]$ direction, the energy barrier of Path III decreases more rapidly than that of Path I. The strain applied along [001] does not change the difference of the energy barriers of Path I and Path III evidently, as shown in Fig. 7(d). Therefore in order to facilitate the diffusion anisotropy in favor of diffusion along $[1\bar{1}0]$, a possible way is to apply tensile strain in $[1\bar{1}0]$.

From Figs. 7(c) and 7(d), consistency can be also found between the calculated energy barriers using NEB method and the predicted ones, especially when the strain is relatively small. Therefore we conclude that the proposed method for predicting the diffusion barrier of adatoms is still applicable to diffusion of oxygen vacancies on oxide surfaces. As a demonstration, we apply this method to estimate the diffusion barrier of Path II under external strain. The values of $(A\Delta\sigma_{11}, A\Delta\sigma_{22})$ is (3.7,−5.9) eV. Accordingly it is expected that the diffusion barrier of Path II increases with strain along $[1\bar{1}0]$, and decreases with strain along [001], as shown in the lower panel of Fig. 7. We can see that within the considered range of strain, the energy barrier of the cross row diffusion of the BOV via hopping mechanism remains the highest and most unfavorable.

V. CONCLUSIONS

In summary, based on the density functional theory, we calculate the formation energy of the three types of the surface oxygen vacancies on the rutile $TiO_2(110)$ under biaxial strain. A phase diagram of the type of EFOV as a function of the external strain ϵ_{11} and ϵ_{22} is established. According to this phase diagram, one can choose the desired EFOV type by tuning the external strain to the corresponding values. Furthermore, the diffusion properties of the surface BOV under external strain are studied. A concerted diffusion mechanism is found for the cross row diffusion of the BOV, which is mediated by the in-plane oxygen vacancy. Tensile strain decreases the energy barriers of diffusion both along and across the bridging oxygen rows. When the strain is applied along the $[1\bar{1}0]$ direction, the efficiency of diffusion in this direction via the concerted mechanism increases much more than that of the diffusion along [001] does. The results are helpful for one to understand the interaction between the external strain and the surface oxygen vacancies of the rutile $TiO_2(110)$ surface. We also suggest that external strain is a potential way to control the physical and chemical properties of the surfaces of the transition metal oxide.

ACKNOWLEDGMENTS

The numerical calculations have been carried out at the Shanghai Supercomputer Center. This work was supported by NSF of China (under Grants No. 10974079 and No. 10874068) and Jiangsu Province (under Grant No. BK2008012), MOE (under Grant No. NCET-09-0461) and MOST of China (under Grants No. 2010CB630705 and No. 2006CB921804).

*Corresponding author. djshu@nju.edu.cn
†Corresponding author. muwang@nju.edu.cn

[1] R. Asahi, T. Morikawa, T. Ohwaki, K. Aoki, and Y. Taga, Science **293**, 269 (2001).
[2] C. T. Campbell, S. C. Parker, and D. E. Starr, Science **298**, 811 (2002).
[3] M. Grätzel, Nature (London) **414**, 338 (2001).
[4] O. Bikondoa, C. L. Pang, R. Ithnin, C. A. Muryn, H. Onishi, and G. Thornton, Nature Mater. **5**, 189 (2006).
[5] G. Lu, A. Linsebigler, and J. T. Yates, J. Phys. Chem. **99**, 7626 (1995).
[6] S. Wendt *et al.*, Surf. Sci. **598**, 226 (2005).
[7] T. L. Thompson and J. T. Yates, Chem. Rev. **106**, 4428 (2006).
[8] C. M. Yim, C. L. Pang, and G. Thornton, Phys. Rev. Lett. **104**, 036806 (2010).
[9] U. Diebold, J. Lehman, T. Mahmoud, M. Kuhn, G. Leonardelli, W. Hebenstreit, M. Schmid, and P. Varga, Surf. Sci. **411**, 137 (1998).
[10] E. Wahlström, N. Lopez, R. Schaub, P. Thostrup, A. Rønnau, C. Africh, E. Lægsgaard, J. K. Nørskov, and F. Besenbacher, Phys.

Rev. Lett. **90**, 026101 (2003).
[11] R. Schaub, E. Wahlstrom, A. Ronnau, E. Laegsgaard, I. Stensgaard, and F. Besenbacher, Science **299**, 377 (2003).
[12] Z. R. Zhang, R. Rousseau, J. L. Gong, S. C. Li, B. D. Kay, Q. F. Ge, and Z. Dohnalek, Phys. Rev. Lett. **101**, 156103 (2008).
[13] G. A. Kimmel and N. G. Petrik, Phys. Rev. Lett. **100**, 196102 (2008).
[14] D. O. Klenov, W. Donner, B. Foran, and S. Stemmer, Appl. Phys. Lett. **82**, 3427 (2003).
[15] H. Kamisaka and K. Yamashita, Surf. Sci. **601**, 4824 (2007).
[16] B. Yang, F. Liu, and M. G. Lagally, Phys. Rev. Lett. **92**, 025502 (2004).
[17] G. H. Lu, M. Cuma, and F. Liu, Phys. Rev. B **72**, 125415 (2005).
[18] N. C. Yu and J. W. Halley, Phys. Rev. B **51**, 4768 (1995).
[19] G. F. Wang and X. Q. Feng, Appl. Phys. Lett. **90**, 231904 (2007).
[20] C. W. Pao, D. J. Srolovitz, and C. V. Thompson, Phys. Rev. B **74**, 155437 (2006).
[21] D. Yu and F. Liu, Nano Lett. **7**, 3046 (2007).
[22] D. J. Shu, S. T. Ge, M. Wang, and N. B. Ming, Phys. Rev. Lett. **101**, 116102 (2008).
[23] Z. Zhang, Q. Ge, S. C. Li, B. D. Kay, J. M. White, and Z. Dohnalek, Phys. Rev. Lett. **99**, 126105 (2007).
[24] X. Cui, B. Wang, Z. Wang, T. Huang, Y. Zhao, J. Yang, and J. Hou, J. Chem. Phys. **129**, 044703 (2008).
[25] D. J. Shu, F. Liu, and X. G. Gong, Phys. Rev. B **64**, 245410 (2001).
[26] J. P. Perdew, K. Burke, and M. Ernzerhof, Phys. Rev. Lett. **77**, 3865 (1996).
[27] G. Kresse and D. Joubert, Phys. Rev. B **59**, 1758 (1999).
[28] P. E. Blöchl, Phys. Rev. B **50**, 17953 (1994).
[29] H. J. Monkhorst and J. D. Pack, Phys. Rev. B **13**, 5188 (1976).
[30] G. Mills, H. Jonsson, and G. K. Schenter, Surf. Sci. **324**, 305 (1995).
[31] V. B. Shenoy, Phys. Rev. B **71**, 094104 (2005).
[32] M. Schmid, W. Hofer, P. Varga, P. Stoltze, K. W. Jacobsen, and J. K. Norskov, Phys. Rev. B **51**, 10937 (1995).
[33] M. D. Rasmussen, L. M. Molina, and B. Hammer, J. Chem. Phys. **120**, 988 (2004).
[34] U. Diebold, Surf. Sci. Rep. **48**, 53 (2003).
[35] T. Ala-Nissila, R. Ferrando, and S. C. Ying, Adv. Phys. **51**, 949 (2002).
[36] L. D. Roelofs, B. J. Greenblatt, and N. Boothe, Surf. Sci. **334**, 248 (1995).
[37] U. Kürpick and T. S. Rahman, Phys. Rev. B **59**, 11014 (1999).